Journal of Solid State Chemistry **162,** 168–175 (2001)
doi:10.1006/jssc.2001.9212, available online at http://www.idealibrary.com IDEAL®

Synthesis, Crystal Structure, and Solid State NMR Spectroscopy of $(C_{10}N_4H_{28})[Zn_6(HPO_4)_2(PO_4)_4]\cdot 2H_2O$, a New Zinc Phosphate with a Layer Structure

Yung-Ping Chiang,* Hsien-Ming Kao,*,[1] and Kwang-Hwa Lii*,†,[1]

*Department of Chemistry, National Central University, Chungli, Taiwan, Republic of China; and †Institute of Chemistry, Academia Sinica, Nankang, Taipei, Taiwan, Republic of China

Received January 16, 2001; in revised form March 29, 2001; accepted April 12, 2001; published online June 11, 2001

IN HONOR OF PROFESSOR PAUL HAGENMULLER ON THE OCCASION OF HIS 80TH BIRTHDAY

A new zinc phosphate, $(C_{10}N_4H_{28})[Zn_6(HPO_4)_2(PO_4)_4]\cdot 2H_2O$, with a layered architecture has been synthesized, for the first time, in the presence of 1,4-bis(3-aminopropyl)piperazine as the structure-directing agent. The structure comprises a network of ZnO_4 and phosphate tetrahedra forming macroanionic layers with eight-membered apertures. Charge compensation is achieved by the quadruply protonated amine occupying interlamellar space and interacts with the inorganic layers via hydrogen bonding. The title compound is related to several other zinc phosphates in framework stoichiometry or crystal structure. Crystal data: $(C_{10}N_4H_{28})[Zn_6(HPO_4)_2(PO_4)_4]\cdot 2H_2O$, triclinic, space group $P\bar{1}$(No. 2), $a = 8.3343(9)$ Å, $b = 12.413(1)$ Å, $c = 17.363(2)$ Å, $\alpha = 75.269(2)^\circ$, $\beta = 78.868(2)^\circ$, $\gamma = 76.270(2)^\circ$, $V = 1670.7(5)$ Å^3, $Z = 2$, $R_1 = 0.0584$, $wR_2 = 0.153$. Proton-decoupled ^{31}P MAS NMR reveals six ^{31}P resonances with nearly equal intensities, which is in good agreement with the six distinct crystallographic phosphorus sites in the framework as indicated from X-ray structural analysis. $^1H \rightarrow {}^{31}P$ CP/MAS is used to obtain more details of the proximity between hydrogen and phosphorus atoms, and in combination with 2D RFDR NMR to assign the six phosphorus sites. © 2001 Elsevier Science

INTRODUCTION

Since the first microporous zinc phosphates with zeolite-like topologies were reported by Gier and Stucky (1), a large number of zincophosphates (ZnPOs) with 1-D, 2-D, and 3-D structures have been synthesized in the presence of organic templates (2). The structural diversity among these ZnPOs is substantial. Most structures are built mainly from tetrahedral of ZnO_4 and PO_4 but examples of ZnO_6 and ZnO_5 subunits are also known (3). Few examples are zeolite-like with fully alternating tetrahedral Zn/P framework topology. In most other compounds, the frameworks are interrupted by the presence of terminal P–OH, P = O, or Zn–OH_2 groups. In addition connectivity between two or more ZnO_4 tetrahedra and nitrogen of the organic amine template being coordinated to zinc can also occur (4–7). The organic cation often has a structure-directing effect, but it is difficult to control or to predict the structure features of the resulting ZnPOs. Indeed, the variety of structures obtainable in this system is one of its most interesting features. We have been interested in the synthesis of phosphates of transition metals or group 13 elements with novel topology (8–10). In the case of zinc we obtained a new zinc phosphate with the same framework stoichiometry as $Zn_3(PO_4)_2(PO_3OH)(H_2DACH)$ and $(H_4TETA)_{0.5}$ $[Zn_3(PO_4)_2(HPO_4)]$ (11, 12), which contain 24- and 16-membered one-dimensional channels respectively, although they adopt quite different crystal structures. Here we report the synthesis and characterization of $(C_{10}N_4H_{28})$ $[Zn_6(HPO_4)_2(PO_4)_4]\cdot 2H_2O$ (designated NCUZn-1) with a 2-D layer structure where 1,4-bis(3-aminopropyl) piperazine acts as the template. Its structure is determined by a combination of single-crystal X-ray diffraction and solid-state ^{31}P NMR techniques.

EXPERIMENTAL

Synthesis and initial characterization. Hydrothermal reaction of $Zn(NO_3)_2\cdot 6H_2O$, H_3PO_4, $H_2C_2O_4\cdot 2H_2O$, 1,4-bis(3-aminopropyl)piperazine (abbreviated to APPIP), and H_2O in the molar ratio of 1 : 3 : 2 : 1.5 : 555 in a Teflon-lined acid digestion bomb at 180°C for 3 days produced colorless long prismatic to acicular crystals of $(C_{10}N_4H_{28})$ $[Zn_6(HPO_4)_2(PO_4)_4]\cdot 2H_2O$ in 77% yield based on Zn. The pH of the reaction mixture before and after crystallization was 2.5 and 3.6, respectively. The bulk product is monophasic as judged by the total consistency of its X-ray powder pattern with that simulated from the atomic coordinates derived from a single-crystal X-ray study.

[1]To whom correspondence should be addressed.

Energy-dispersive X-ray fluorescence spectroscopy of several colorless crystals confirms the presence of Zn and P. Elemental analysis of C, H, and N contents is consistent with the stoichiometry. (Anal. found: C, 9.97; H, 2.87; N, 4.55%. Calcd: C, 9.97; H, 2.85; N, 4.65%.) We have also carried out retrosyntheses, excluding oxalic acid as a reactant; the resulting product is $(C_{10}N_4H_{28})_{0.5}[Zn(HPO_4)_2]\cdot 2H_2O$ (13). Thermogravimetric analysis (TGA) in a flowing oxygen atmosphere in the temperature range of 40–950°C with a heating rate of 5°C min^{-1} showed weight loss in several overlapping steps (Fig. 1). The observed mass loss between 40 and 300°C (3.13%) is close to the calculated value (2.99%) for the loss of the guest water molecules. Powder X-ray diffraction of the samples that had been heated in air and then cooled to RT revealed that the compound retained its structure at 250°C. The next mass loss at about 400°C, which is not well resolved from the final steps, is probably due to dehydration of the hydrogen phosphate groups and deprotonation of the amine cations. The final steps correspond to the release of organic components, giving $Zn_2P_2O_7$ as the final decomposition product as indicated by powder X-ray diffraction. The observed total weight loss of 24.22% agrees well with the calculated value (24.11%) for the loss of 1 APPIP and 5 H_2O molecules. An ion-exchange experiment was performed by stirring $(C_{10}N_4H_{28})$ $[Zn_6(HPO_4)_2(PO_4)_4]\cdot 2H_2O$ with 1 N $NaOH_{(aq)}$ at room temperature for 3 h. The X-ray powder pattern of the reaction product was identical with that of the reactant, indicating that the organic cations were not replaced by Na^+. In contrast, $Zn_3(PO_4)_2(PO_3OH)$ (H_2DACH) reacts readily with sodium cations in a slightly basic solution to give $Na_3Zn_3(PO_4)_3\cdot 4H_2O$, which is isostructural with sodalite, $Na_3Al_3Si_3O_{12}\cdot 4H_2O$ (11).

Single-crystal X-ray diffraction. A colorless long prismatic crystal of $(C_{10}N_4H_{28})[Zn_6(HPO_4)_2(PO_4)_4]\cdot 2H_2O$ with the dimensions $0.04\times 0.08\times 0.5\ mm^3$ was mounted on a Siemens Smart-CCD diffractometer equipped with a normal focus, 3-kW sealed-tube X-ray source (Mo$K\alpha$, 0.71073 Å). Intensity data were collected in 1271 frames with increasing ω (width of 0.30° per frame). Octants collected and $2\theta_{max}$ were as follows: $-10\le h\le 11$, $-16\le k\le 16$, $-22\le l\le 22$, 56.7°. The number of measured reflections, unique reflections, and observed unique reflections $[I>2\sigma(I)]$ were 17650, 7883, and 6478, respectively. Empirical absorption corrections were performed by using the SADABS program for Siemens area detector ($T_{min,\,max}$: 0.630, 0.942). On the basis of statistics for intensity distribution and successful solution and refinement of the structure, the space group was determined to be $P\bar{1}$ (No. 2). The structure was solved by direct methods. The Zn and P atoms were first located, and the C, N, and O atoms were found in difference Fourier maps. Hydrogen atoms could not be located in the crystal structure determination. Bond-valence sum calculations (14) indicate that O(25) and O(26) are water oxygen atoms, and O(20) and O(24) are hydroxo oxygen atoms and, therefore, P(5) and P(6) form HPO_4^{2-} groups. The N atom and the C atom next to it within either of the two 3-aminopropyl groups in the organic cation gave nonpositive definite values when they were refined with anisotropic displacement parameters. Their large thermal parameters and the unreasonable C–N and C–C bond lengths and bond angles indicate that the 3-aminopropyl groups are disordered and an organic cation is loosely bound in the structure. A satisfactory model to describe the disordering of the end groups was not found. The final cycles of least-squares refinement against F^2 including the atomic coordinates of all atoms, isotropic thermal parameters for the two N and two C atoms in the 3-aminopropyl groups, and anisotropic thermal parameters for all other atoms converged at $R_1=0.0584$ and $wR_2=0.1531$. Secondary extinction corrections were applied. The final difference Fourier maps revealed large residual electron densities (4.5 and 2.2 e $Å^{-3}$) near N(1) and C(1) and smaller peaks (2.2 and 1.7 e $Å^{-3}$) near N(4) and C(10), indicating that one of the end groups is disordered to an extent greater than that of the other. Structure solution and refinement were performed using SHELXTL programs (15).

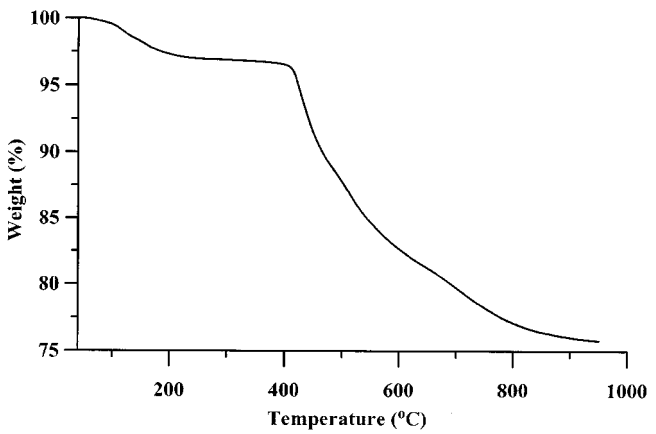

FIG. 1. Thermogravimetric analysis of $(C_{10}N_4H_{28})$ $[Zn_6(HPO_4)_2(PO_4)_4]\cdot 2H_2O$ in flowing oxygen at 5°C min^{-1}.

Solid state NMR measurements. All ^{31}P NMR spectra were recorded on a Bruker AVANCE-400 spectrometer with a standard Bruker double-tuned 4-mm probe at a ^{31}P resonance frequency of 161.73 MHz. Pulse lengths of 2.5 μs (90° flip angle) and recycle delays of 40 s were found to be adequate for quantitatively reliable ^{31}P magic angle spinning (MAS) NMR spectra under conditions of high-power proton decoupling. The Hartmann–Hahn conditions for $^1H\rightarrow{}^{31}P$ cross-polarization (CP) experiments were set on $(NH_4)_2HPO_4$. ^{31}P CP/MAS NMR spectra were recorded as a function of the contact time ranging from 0.1 to

20 ms. Chemical shifts of ^{31}P were externally referenced to 85% H_3PO_4.

Two-dimensional ^{31}P radiofrequency dipolar recoupling (RFDR) NMR experiments were performed at a spinning speed of 12.5 kHz with controlled stability to within $\pm$ 1 Hz (16). Typically 80 increments of t_1 were accumulated. The mixing time, t_m, was varied between 1 and 20 ms. The TPPI method was used to obtain phase-sensitive spectra in both dimensions (17).

RESULTS AND DISCUSSION

Description of the structure. The crystallographic data are summarized in Table 1. The atomic coordinates and selected bond lengths and angles are given in Tables 2 and 3, respectively. The asymmetric unit consists of 52 distinct nonhydrogen atoms, all of which are at general positions in the unit cell. There is one quadruply protonated APPIP molecule per asymmetric unit. There are six distinct Zn and six P atoms. Figure 2 shows the connectivity between the Zn–O and P–O tetrahedra. This phase is a new zincophosphate with a two-dimensional character based on sheets of ZnO_4, PO_4, and HPO_4 tetrahedra fused together via Zn–O–P and Zn–O–Zn bonds. A view of a section of a sheet is shown in Fig. 3a, and the complete crystal structure in Fig. 4. All zinc atoms make four Zn–O–P linkages to nearby phosphorus atoms. All but two oxygen atoms are

TABLE 1
Crystallographic Data for
$(C_{10}N_4H_{28})[Zn_6(HPO_4)_2(PO_4)_4]\cdot 2H_2O$

Formula weight	1204.45
Crystal system	Triclinic
Space group	$P\bar{1}$
a, Å	8.3343(9)
b, Å	12.413(1)
c, Å	17.363(2)
α, °	75.269(2)
β, °	78.868(2)
γ, °	76.270(2)
Volume, Å^3	1670.7(5)
Z	2
D_{calc}, g cm^{-3}	2.394
μ, mm^{-1}	4.63
T, °C	22
λ, Å	0.71073
Number of unique data [$I > 2\sigma(I)$]	6478
Number of variables	450
R_1[a]	0.0584
wR_2[b]	0.1531
Goodness-of-fit	1.047

[a] $R_1 = \sum ||F_o| - |F_c|| / \sum |F_o|$ for $F_o > 4\sigma(F_o)$.
[b] $wR_2 = \{\sum [w(|F_o|^2 - |F_c|^2)^2] / [w(|F_o|^2)^2]\}^{1/2}$ for all data, where $w = 1/[\sigma^2(F_o^2) + (0.0795P)^2 + 15.82P]$ and $P = [\mathrm{Max}(F_o^2, 0) + 2F_c^2]/3$.

TABLE 2
Atomic Coordinates and Thermal Parameters (Å^2) for
$(C_{10}N_4H_{28})[Zn_6(HPO_4)_2(PO_4)_4]\cdot 2H_2O$

Atom	x	y	z	U_{eq}[a]
Zn(1)	0.20203(9)	0.10771(6)	0.22112(4)	0.0202(2)
Zn(2)	0.09786(9)	0.39057(6)	0.23152(5)	0.0222(2)
Zn(3)	0.69963(9)	0.08961(6)	0.25442(4)	0.0209(2)
Zn(4)	0.59682(9)	0.37137(6)	0.26724(4)	0.0212(2)
Zn(5)	−0.0056(1)	−0.17552(7)	0.54630(4)	0.0243(2)
Zn(6)	−0.39267(9)	0.31795(6)	0.04093(4)	0.0215(2)
P(1)	0.3886(2)	0.5115(1)	0.1302(1)	0.0199(3)
P(2)	−0.1090(2)	0.2748(1)	0.15052(9)	0.0188(3)
P(3)	−0.0290(2)	−0.0158(1)	0.3679(1)	0.0198(3)
P(4)	0.3403(2)	0.2052(1)	0.33340(9)	0.0189(3)
P(5)	−0.1830(2)	0.4258(1)	0.3820(1)	0.0221(3)
P(6)	0.5536(2)	0.0600(1)	0.1125(2)	0.0206(3)
O(1)	0.5344(6)	0.4926(4)	0.1776(3)	0.031(1)
O(2)	−0.3761(6)	0.3701(4)	−0.0749(3)	0.028(1)
O(3)	−0.5879(6)	0.4186(5)	0.0830(3)	0.033(1)
O(4)	0.2237(6)	0.5113(4)	0.1886(3)	0.026(1)
O(5)	0.0283(1)	0.1676(4)	0.1521(3)	0.029(1)
O(6)	0.7487(6)	0.2451(4)	0.2218(3)	0.025(1)
O(7)	−0.1788(6)	0.3091(4)	0.0707(3)	0.027(1)
O(8)	−0.0477(6)	0.3752(4)	0.1622(3)	0.030(1)
O(9)	0.1348(6)	−0.0105(4)	0.3100(3)	0.030(1)
O(10)	0.8359(7)	−0.0268(4)	0.3235(3)	0.030(1)
O(11)	0.0069(6)	−0.1254(4)	0.4311(3)	0.028(1)
O(12)	0.0914(7)	−0.0881(5)	0.5955(3)	0.036(1)
O(13)	0.2248(6)	0.2335(4)	0.2671(3)	0.026(1)
O(14)	0.4036(6)	0.3119(4)	0.3302(3)	0.028(1)
O(15)	0.4792(6)	0.1063(4)	0.3183(3)	0.030(1)
O(16)	−0.2413(6)	−0.1712(5)	0.5839(3)	0.031(1)
O(17)	0.6745(8)	0.4139(9)	0.3482(5)	0.075(3)
O(18)	0.127(1)	−0.3275(5)	0.5517(4)	0.062(2)
O(19)	−0.0371(9)	0.4511(6)	0.3198(4)	0.054(2)
O(20)	−0.2493(9)	0.5336(5)	0.4202(4)	0.047(2)
O(21)	0.3934(6)	0.0300(5)	0.1614(3)	0.033(1)
O(22)	0.6959(6)	0.0328(5)	0.1609(3)	0.032(1)
O(23)	−0.4734(8)	0.1790(5)	0.0614(4)	0.048(2)
O(24)	0.6079(7)	−0.0258(5)	0.0533(3)	0.039(1)
O(25)	0.199(1)	0.4224(9)	0.4494(6)	0.093(3)
O(26)	0.093(1)	0.0366(7)	0.0384(4)	0.063(2)
N(1)	−0.778(2)	0.430(1)	−0.0411(8)	0.092(4)[b]
N(2)	−0.075(1)	0.2735(7)	−0.1973(7)	0.068(3)
N(3)	−0.260(2)	0.2466(9)	−0.3136(7)	0.085(4)
N(4)	−0.593(5)	0.123(3)	−0.444(2)	0.26(1)[b]
C(1)	−0.782(2)	0.297(1)	−0.0433(9)	0.087(4)[b]
C(2)	−0.868(2)	0.325(1)	−0.1331(9)	0.082(4)
C(3)	−0.947(2)	0.232(1)	−0.1313(9)	0.077(4)
C(4)	−0.189(1)	0.1909(7)	−0.1777(7)	0.052(2)
C(5)	−0.993(2)	0.281(1)	−0.2766(9)	0.077(4)
C(6)	−0.332(1)	0.2298(8)	−0.2236(7)	0.053(2)
C(7)	−0.117(2)	0.321(1)	−0.3295(6)	0.062(3)
C(8)	−0.377(2)	0.290(1)	−0.369(1)	0.099(5)
C(9)	−0.501(2)	0.207(2)	−0.378(2)	0.15(1)
C(10)	−0.428(6)	0.161(4)	−0.456(3)	0.26(2)[b]

[a] U_{eq} is defined as one-third of the trace of the orthogonalized U_{ij} tensor.
[b] The atom is refined with an isotropic temperature factor.

TABLE 3
Selected Interatomic Distances (Å) and Bond Angles (°) for $(C_{10}N_4H_{28})[Zn_6(HPO_4)_2(PO_4)_4]\cdot 2H_2O$

		Distances	
Zn(1)–O(5)	1.947(5)	Zn(1)–O(9)	1.937(5)
Zn(1)–O(13)	1.986(5)	Zn(1)–O(21)	1.921(5)
Zn(2)–O(4)	1.944(5)	Zn(2)–O(8)	1.936(5)
Zn(2)–O(13)	1.991(5)	Zn(2)–O(19)	1.924(6)
Zn(3)–O(6)	1.985(5)	Zn(3)–O(10)	1.919(5)
Zn(3)–O(15)	1.949(5)	Zn(3)–O(22)	1.936(5)
Zn(4)–O(1)	1.925(5)	Zn(4)–O(6)	1.995(5)
Zn(4)–O(14)	1.951(5)	Zn(4)–O(17)	1.889(6)
Zn(5)–O(11)	1.927(5)	Zn(5)–O(12)	1.928(5)
Zn(5)–O(16)	1.940(5)	Zn(5)–O(18)	1.936(6)
Zn(6)–O(2)	1.937(5)	Zn(6)–O(3)	1.945(5)
Zn(6)–O(7)	1.921(5)	Zn(6)–O(23)	1.923(6)
P(1)–O(1)	1.537(5)	P(1)–O(2)	1.530(5)
P(1)–O(3)	1.534(5)	P(1)–O(4)	1.543(5)
P(2)–O(5)	1.533(5)	P(2)–O(6)	1.576(5)
P(2)–O(7)	1.527(5)	P(2)–O(8)	1.526(5)
P(3)–O(9)	1.536(5)	P(3)–O(10)	1.531(5)
P(3)–O(11)	1.523(5)	P(3)–O(12)	1.518(5)
P(4)–O(13)	1.561(5)	P(4)–O(14)	1.523(5)
P(4)–O(15)	1.512(5)	P(4)–O(16)	1.524(5)
P(5)–O(17)	1.474(6)	P(5)–O(18)	1.501(6)
P(5)–O(19)	1.498(6)	P(5)–O(20)	1.579(6)
P(6)–O(21)	1.509(5)	P(6)–O(22)	1.509(5)
P(6)–O(23)	1.508(6)	P(6)–O(24)	1.594(5)
N(1)–C(1)	1.67(2)	N(2)–C(3)	1.62(1)
N(2)–C(4)	1.49(1)	N(2)–C(5)	1.40(2)
N(3)–C(6)	1.54(2)	N(3)–C(7)	1.61(2)
N(3)–C(8)	1.42(2)	N(4)–C(10)	1.52(5)
C(1)–C(2)	1.76(2)	C(2)–C(3)	1.45(2)
C(4)–C(6)	1.48(1)	C(5)–C(7)	1.43(2)
C(8)–C(9)	1.66(2)	C(9)–C(10)	1.56(5)
		Angles	
P(1)–O(1)–Zn(4)	128.5(3)	P(1)–O(2)–Zn(6)	132.6(3)
P(1)–O(3)–Zn(6)	133.2(3)	P(1)–O(4)–Zn(2)	129.3(3)
P(2)–O(5)–Zn(1)	129.1(3)	P(2)–O(6)–Zn(3)	120.5(3)
P(2)–O(6)–Zn(4)	118.6(3)	Zn(3)–O(6)–Zn(4)	120.3(2)
P(2)–O(7)–Zn(6)	134.2(3)	P(2)–O(8)–Zn(2)	133.8(3)
P(3)–O(9)–Zn(1)	131.8(3)	P(3)–O(10)–Zn(3)	128.9(3)
P(3)–O(11)–Zn(5)	139.3(3)	P(3)–O(12)–Zn(5)	135.9(4)
P(4)–O(13)–Zn(1)	118.3(3)	P(4)–O(13)–Zn(2)	121.1(3)
Zn(1)–O(13)–Zn(2)	120.6(2)	P(4)–O(14)–Zn(4)	131.8(3)
P(4)–O(15)–Zn(3)	135.4(3)	P(4)–O(16)–Zn(5)	133.2(3)
P(5)–O(17)–Zn(4)	148.4(5)	P(5)–O(18)–Zn(5)	135.4(4)
P(5)–O(19)–Zn(2)	138.0(4)	P(6)–O(21)–Zn(1)	135.5(3)
P(6)–O(22)–Zn(3)	126.7(3)	P(6)–O(23)–Zn(6)	140.4(4)

two-bonded, with the exception of O(6) and O(13) being bonded to two Zn and one P atoms, and thus providing Zn(1)–O(13)–Zn(2) and Zn(3)–O(6)–Zn(4) linkages in the structure, a feature that has been observed in several ZnPOs reported earlier. In all cases the Zn–O–Zn linkages are always accompanied by the trigonal coordination of the bridging oxygen atoms. The third coordination is always to one P cation. The trigonal coordination of the oxygen atom in the Zn–O–Zn linkage is apparently an electrostatic

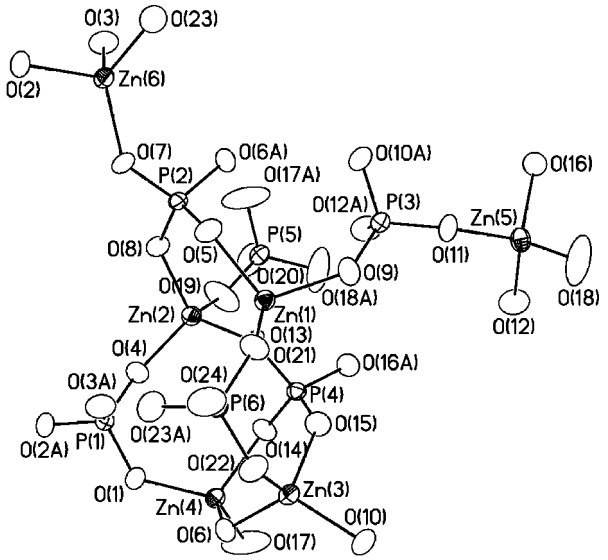

FIG. 2. ORTEP plot of $(C_{10}N_4H_{28})[Zn_6(HPO_4)_2(PO_4)_4]\cdot 2H_2O$ showing the connectivity between the Zn–O and P–O tetrahedra. Thermal ellipsoids are shown at 50% probability.

valence requirement of the bridging oxygen atoms. The coordination geometries of O(6) and O(13) in $(C_{10}N_4H_{28})[Zn_6(HPO_4)_2(PO_4)_4]\cdot 2H_2O$ approximate an isosceles triangle. Each of these four ZnO_4 tetrahedron with Zn–O–Zn bonding has a wide spread of Zn–O bond lengths with the longest bond being associated with a three-coordinate oxygen atom. The Zn–O bond lengths in $Zn(5)O_4$ and $Zn(6)O_4$, which are not involved in Zn–O–Zn linkage, are considerably more regular. Bond-valence sum calculations indicate that the long P(5)–O(20) and P(6)–O(24) bonds are parts of the P–OH groups. The P–O bond lengths in $P(1)O_4$ and $P(3)O_4$ are regular. The P(2)–O and P(4)–O tetrahedra are less regular with the longest bonds again being associated with three-coordinate oxygen atoms.

Figure 3b shows the network structure of a layer in $(C_{10}N_4H_{28})[Zn_6(HPO_4)_2(PO_4)_4]\cdot 2H_2O$. The basic building unit is a four-membered ring fused through a three-coordinate oxygen atom to form strips along the *a* axis. The $Zn(5)O_4$ or $Zn(6)O_4$ unit caps such a strip, forming a tube-like arrangement, and connects such tubes in two dimensions forming a layer. Each layer consists of two types of eight-membered rings, both of which are formed of eight alternating Zn- and P-centered tetrahedra (four Zn and four P). One eight-membered ring is squashed and the other is more regular. There is only one crystallographically distinct layer that is parallel to the *bc* plane. Each layer may also be considered to be formed from infinite chains along the *a* axis built up from dimeric units Zn_2O_7 and phosphate tetrahedra, fused through Zn–O–P bonds. These infinite chains are linked into continuous sheets via $Zn(5)O_4$ and $Zn(6)O_4$ tetrahedra through Zn–O–P bonds. The

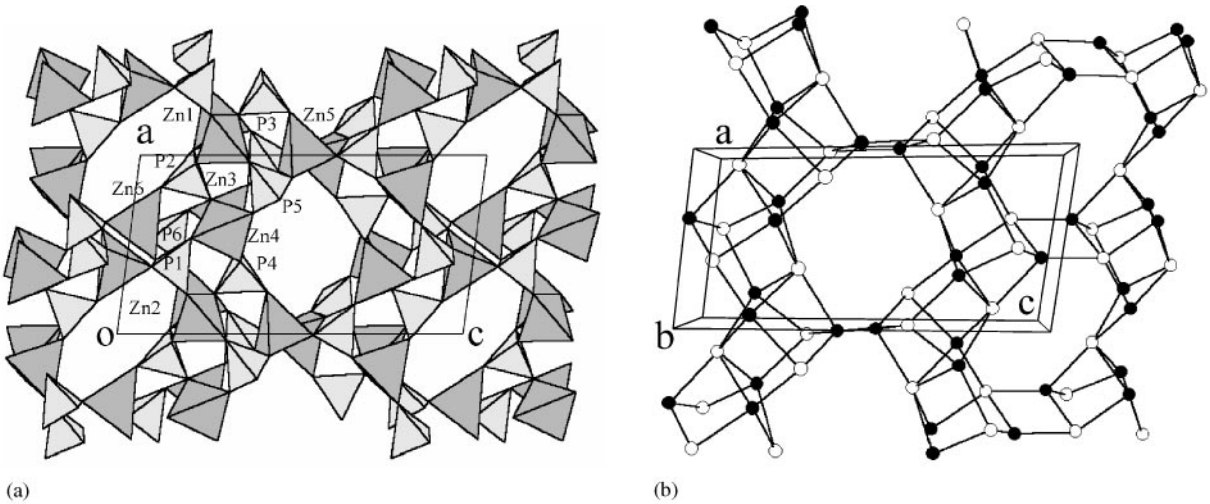

FIG. 3. (a) Section of a sheet in $(C_{10}N_4H_{28})[Zn_6(HPO_4)_2(PO_4)_4]\cdot 2H_2O$. ZnO_4 tetrahedra are dark gray and phosphate tetrahedral are light gray. (b) The network structure of a layer. Only the Zn (solid circles) and P (open circles) atoms are shown.

tetrahedra pointing toward the interlayer space are $(PO_3OH)^{2-}$ groups. Adjacent sheets are aligned such that two types of straight channels along the *b* axis are formed. The organic cations and water molecules occupy space between the layers. Each N atom of the organic cation is within 3 Å of one to three framework O atoms; this distance is indicative of N–H $\cdots$ O hydrogen bonding. The water molecule $H_2O(26)$ is located within the squashed eight-membered ring channel, while the other water molecule $H_2O(25)$ and the organic cation are near the rim of the regular channel. The water molecules also participate in hydrogen bonding with the framework, as indicated from short O $\cdots$ O distances. O(25) has a thermal parameter considerably larger than that of O(26) because the latter is involved in hydrogen bonding with more oxygen atoms.

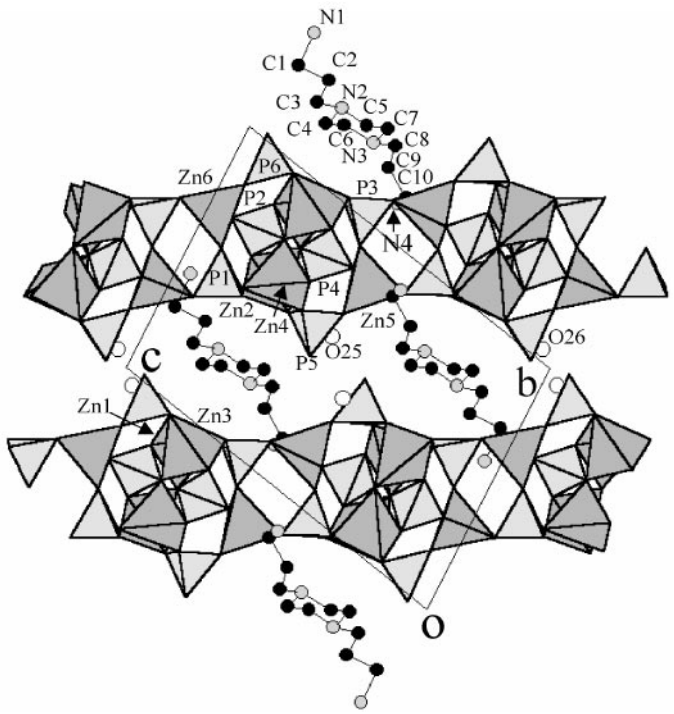

FIG. 4. Structure of $(C_{10}N_4H_{28})[Zn_6(HPO_4)_2(PO_4)_4]\cdot 2H_2O$ viewed along the *a* axis. Solid and stippled circles are C and N atoms of H_4APPIP cations, respectively. Open circles are water oxygen atoms.

We note that the structure of $(C_{10}N_4H_{28})[Zn_6(HPO_4)_2(PO_4)_4]\cdot 2H_2O$ is closely related to that of $(H_3DETA)[Zn_4(PO_4)_3(HPO_4)]\cdot H_2O$ (DETA = diethylenetriamine) (18). The latter consists of sheets of zincophosphate that are connected by HPO_4 groups to form a 3-D framework with intersecting eight-membered ring channels. Each sheet is formed from infinite chains built up from dimeric units Zn_2O_7 and phosphate tetrahedra, fused through Zn–O–P bonds in the same way as that in $(C_{10}N_4H_{28})[Zn_6(HPO_4)_2(PO_4)_4]\cdot 2H_2O$. These infinite chains are sheathed with discrete ZnO_4 tetrahedra and are linked into sheets via HPO_4 tetrahedra. In contrast the infinite chains in $(C_{10}N_4H_{28})[Zn_6(HPO_4)_2(PO_4)_4]\cdot 2H_2O$ are linked into sheets through ZnO_4 tetrahedra with the organic cations between the sheets. It is interesting that $(C_{10}N_4H_{28})[Zn_6(HPO_4)_2(PO_4)_4]\cdot 2H_2O$, $Zn_3(PO_4)_2(PO_3OH)(H_2DACH)$ (DACH = diaminocyclohexane) (11) and $(H_4TETA)_{0.5}[Zn_3(PO_4)_2(HPO_4)]$ (TETA = triethylenetetramine) (12) have the same framework stoichiometry. Although the former two structures are built up from corner-sharing ZnO_4, PO_4, and HPO_4 moieties and characterized by the presence of Zn–O–Zn linkages, the connectivity of the building units in $Zn_3(PO_4)_2(PO_3OH)$

(H_2DACH) results in a 3-D framework structure with gigantic pores of 24 tetrahedra. No Zn–O–Zn linkages are present in the 3-D framework structure of $(H_4TETA)_{0.5}[Zn_3(PO_4)_2(HPO_4)]$. The organic species APPIP, DACH, and TETA direct the formation of completely different structures. This work shows that the inorganic frameworks adopt themselves to the organic amines according to their shapes and characters.

In the course of this work a new layered zinc phosphate with composition $(C_6H_{17}N_3)[Zn_3(HPO_4)(PO_4)_2]\cdot H_2O$ (designated UiO-27) was reported by Kongshaug *et al.* (19). It was prepared by a hydrothermal synthesis using 1-(2-aminoethyl)piperazine as the structure-directing agent. The compound crystallizes in the monoclinic space group $P2_1/c$ and its structure was determined by powder X-ray diffraction. The zinc phosphate layers are similar to those in $(C_{10}N_4H_{28})[Zn_6(HPO_4)_2(PO_4)_4]\cdot 2H_2O$. Rao *et al.* reported in a review article a new zinc phosphate with the composition $(H_2APPIP)[Zn_3(HPO_4)(PO_4)_2]$ (20). Its inorganic layers appear the same as those in $(C_{10}N_4H_{28})[Zn_6(HPO_4)_2(PO_4)_4]\cdot 2H_2O$. However, the organic amine is diprotonated and there are two APPIP molecules per $[Zn_6(HPO_4)_2(PO_4)_4]$ unit.

^{31}P MAS NMR. Figure 5 shows the proton decoupled ^{31}P MAS NMR spectra of $(C_{10}N_4H_{28})[Zn_6(HPO_4)_2(PO_4)_4]\cdot 2H_2O$, together with the deconvoluted spectrum shown in dashed lines. Six ^{31}P resonances at 6.6, 5.5 (with a shoulder at approx. 5.8), 4.9, 4.1, 1.6, and -0.5 ppm, labeled as A, B, C, D, E, and F, respectively, are observed. These values agree well with chemical shift range found for other ZnPOs reported in the literature. For example, two signals at 5.4 and 3.2 ppm are observed for $(H_2N_2C_6H_{16})_2[Zn_6(H_2O)_8(HPO_4)_4(HPO_3O)_4]$ (21), and three signals at 1.6, -1.1, and -3.3 ppm for $(C_2H_8N)_8[Zn_8(HPO_4)_8(H_2PO_4)_8]\cdot 4H_2O$ (22). The six signals for the title compound have nearly equal intensities, which is in good agreement with six distinct phosphorus sites in the framework as indicated from X-ray structural analysis. These six resonances may be classified into two groups by their chemical shifts, namely, the four resonances at 6.6, 5.5, 4.9, and 4.1 ppm (A to D) and the two resonances at 1.6 and -0.5 ppm (E and F). The shoulder at 5.8 ppm and the peak at 5.5 ppm are no longer resolved as the sample temperature is increased to 350 K, indicating that the two resonances are from phosphorus atoms in very similar environments.

Variable contact time $^1H \rightarrow {}^{31}P$ CP experiments for probing the proximity of the protons in water and the template molecules to framework phosphorous atoms were performed. The contact time dependences of the six ^{31}P signal intensities at room temperature are shown in Fig. 6 and were analyzed according to the equation (23):

$$M(t) = C[\exp(-t/T_{1\rho}(\mathrm{H})) - \exp(-t/T_{\mathrm{HP}})] \times (1 - T_{\mathrm{HP}}/T_{1\rho}(\mathrm{H}))^{-1}, \quad [1]$$

where $M(t)$ is the signal intensity, C is a constant of proportionality, $T_{1\rho}(H)$ is the ^{1}H spin–lattice relaxation time in the rotating frame, and T_{HP} is the cross-relaxation time between the ^{1}H and ^{31}P spins. The difference in ^{31}P signal intensities obtained from CP generally indicates different T_{HP} values for the corresponding phosphorus species. T_{HP} is related to the strength of the dipolar coupling between ^{1}H and ^{31}P nuclei. Variations in T_{HP} result from more or less efficient polarization transfers due to differences in dipolar coupling between the nearby proton spins and the corresponding phosphorus species. Figure 6 shows the contact time dependence of the six ^{31}P signal intensities. The experimental data are fitted to Eq. [1] and the results are listed in

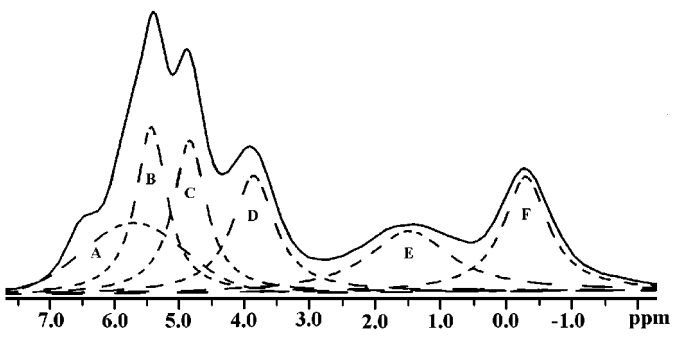

FIG. 5. Proton-decoupled ^{31}P MAS NMR spectrum of as-synthesized $(C_{10}N_4H_{28})[Zn_6(HPO_4)_2(PO_4)_4]\cdot 2H_2O$ with its deconvolution shown in dashed lines.

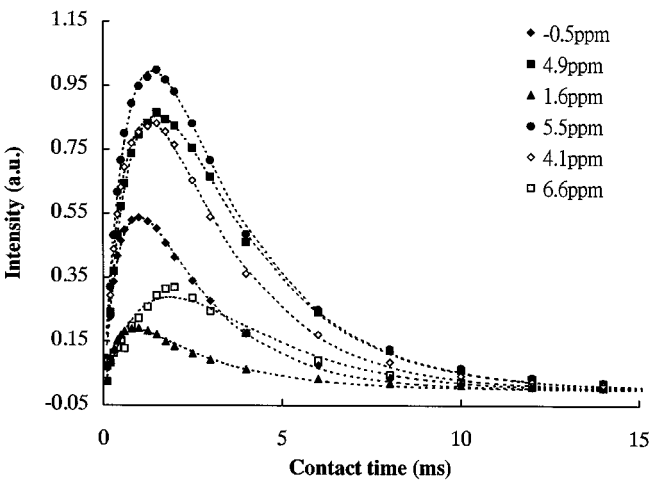

FIG. 6. The evolution of $^1H \rightarrow {}^{31}P$ CP signal intensities as a function of the contact time, obtained at room temperature. The dashed lines are calculated using Eq. [1] with the parameters in Table 4. ◆, -0.5 ppm; ▲, 1.6 ppm; ◇, 4.1 ppm; ■, 4.9 ppm; ●, 5.5 ppm; □, 6.6 ppm.

TABLE 4
Fitted Parameters of $^1H \rightarrow {}^{31}P$ Cross Polarization (see Fig. 5) at Room Temperature

	^{31}P sites (ppm)					
	6.6	5.5	4.9	4.1	1.6	−0.5
T_{HP} (ms)	1.88	0.82	0.99	0.69	0.44	0.56
$T_{1\rho}$ (H) (ms)	1.88	2.62	2.58	2.45	2.39	2.08

Table 4. The cross-relaxation time T_{HP} values are 1.88, 0.82, 0.99, 0.69, 0.44, and 0.56 ms for the 6.6, 5.5, 4.9, 4.1, 1.6, and −0.5 ppm resonances, respectively. The relatively smaller T_{HP} values for the resonances at 1.6 and −0.5 ppm (E and F) indicate that these two phosphorus atoms have very close hydrogen atoms to give rise to a fast transfer of magnetization due to a large ^1H–^{31}P dipolar interaction. These two resonances can be assigned to HPO_4^{2-} groups. The broad resonance E is assigned to P(5) because $HP(5)O_4^{2-}$ forms hydrogen bonds with the mobile water molecule $H_2O(25)$. Other phosphorus sites do not have nearby proton spins that are rigid and close enough to cause such efficient CP signal transfer. The resonance at 6.6 ppm has a considerably large T_{HP} value indicative of the absence of close hydrogen atoms. The CP signal transfer for the B, C, and D sites are ascribed to the hydrogen bonding between the phosphate and the organic template.

In order to correlate ^{31}P chemical shifts and crystallographic sites, we have also performed an RFDR NMR experiment, which is a simple magnetization exchange experiment based on ^{31}P–^{31}P homonuclear dipolar couplings. In RFDR NMR experiments, the dipolar coupling strength between homonuclear spin pairs manifests itself in the intensities of the corresponding cross peaks. Since the dipolar coupling is very sensitive to the distance between the nuclei of interest, an experiment using these couplings should provide results analogous to those from X-ray diffraction. Two-dimensional RFDR magnetization transfer experiments have been performed at different mixing times. With the 2D RFDR experiment only cross peaks between (B, C) and (E, F) are observed at a mixing time of 9.6 ms (Fig. 7). We can assign (B, C) to (P(2), P(4)) sites, as indicated from the distances between the nearest-neighboring phosphorus atoms in Table 5. The overlapping signals on the diagonal for A to D peaks make the assignment difficult. However, it provides direct evidence of the connection between (P(5), P(6)) and (P(2), P(4)) groups. The resonances at 5.5 and 4.9 ppm (B and C) can be assigned to P(2) and P(4), respectively, because the B site experiences a disordered environment caused by the template molecule. In addition, the longer distance between P(2) and P(5), as compared with that between P(2) and P(6), gives a cross peak at weaker

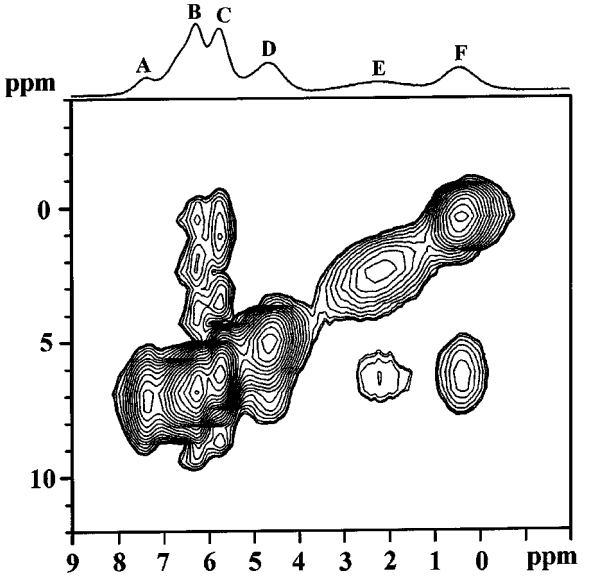

FIG. 7. ^{31}P 2D RFDR spectrum of $(C_{10}N_4H_{28})$ $[Zn_6(HPO_4)_2(PO_4)_4]\cdot 2H_2O$ for a mixing time of $t_m = 9.6$ ms.

intensity, as indicated in Fig. 7. In a similar way, A and D can be assigned to P(1) and P(3), respectively, based on the linewidth of peak A being significantly larger than that of peak D (see Fig. 5). In summary, the resonances from A to F are assigned to P(1), P(2), P(4), P(3), P(5), and P(6), respectively.

^{31}P double-quantum (DQ) NMR experiments based on the BABA sequence (24) to investigate the connectivities between these phosphorus sites have also been performed. Unfortunately, we found that there was an interference between the ^{31}P dipolar recoupling scheme and the proton decoupling that caused the distortions in the spectrum. This interference is known to result from the Hartmann–Hahn match between the DQ and the decoupling sequence. They can be avoided, if the decoupling field strength is at least three times higher than the RF field strength of the BABA sequence. However this condition is difficult to achieve.

TABLE 5
Nearest-Neighbor Distances between Phosphorus Atoms within a 5.5-Å Sphere

	P(1)	P(2)	P(3)	P(4)	P(5)	P(6)
P(1)	4.61	4.54		4.53		
P(2)	4.54		4.55	(5.19, 5.16)	4.75	4.55
P(3)		4.55	4.84	4.46		
P(4)	4.54	(5.16, 5.19)	4.46		4.63	4.50
P(5)		4.75		4.63		
P(6)		4.55		4.54		4.83

In conclusion, a new zinc phosphate with a sheet structure has been synthesized and structurally characterized. Its structure is compared with that of several other zinc phosphates that have the same framework stoichiometry or a related crystal structure. Different organic amines direct the formation of completely different structures. Proton-decoupled ^{31}P MAS NMR reveals six ^{31}P resonances than can be assigned unambiguously by a combination of X-ray structural analysis, $^1H \rightarrow {}^{31}P$ CP/MAS, and ^{31}P 2D RFDR NMR techniques.

Supporting information available. Tables of complete crystal data, atomic coordinates, bond distances and angles, anisotropic thermal parameters, and observed and calculated structure factors are available.

ACKNOWLEDGMENTS

The authors thank the National Science Council and Chinese Petroleum Co. for financial support, Ms. F.-L. Liao and Professor S.-L. Wang at National Tsing Hua University for X-ray data collection, and Ms. R.-R. Wu at National Cheng Kung University for acquiring the NMR spectra. H.M.K. also thanks Dr. R. Graf for his helpful discussion on double-quantum NMR data.

REFERENCES

1. T. E. Gier and G. D. Stucky, *Nature* **349,** 508 (1991).
2. W. Liu, Y. Liu, Z. Shi, and W. Pang, *J. Mater. Chem.* **10,** 1451 (2000), and references therein.
3. W. T. A. Harrison, J. T. Vaughey, L. L. Dussack, A. J. Jacobson, T. E. Martin, and G. D. Stucky, *J. Solid State Chem.* **114,** 151 (1995).
4. T. Song, M. B. Hursthouse, J. Chen, J. Xu, K. M. A. Malik, R. H. Jone, R. Xu, and J. M. Thomas, *Adv. Mater.* **6,** 679 (1994).
5. W. T. A. Harrison, T. M. Nenoff, M. M. Eddy, T. E. Martin, and G. D. Stucky, *J. Mater. Chem.* **2,** 1127 (1992).
6. S. Neeraj, S. Natarajan, and C. N. R. Rao, *New. J. Chem.* **23,** 303 (1999).
7. R. Vaidhyanathan, S. Natarajan, and C. N. R. Rao, *J. Mater. Chem.* **9,** 2789 (1999).
8. K.-H. Lii, Y.-F. Huang, V. Zima, C.-Y. Huang, H.-M. Lin, Y.-C. Jiang, F.-L. Liao, and S.-L. Wang, *Chem. Mater.* **10,** 2599 (1998).
9. K.-H. Lii and Y.-F. Huang, *Inorg. Chem.* **38,** 1348 (1999).
10. C.-Y. Chen, F.-R. Lo, H.-M. Kao, and K.-H. Lii, *Chem. Commun.* 1061 (2000).
11. G.-Y. Yang and S. C. Sevov, *J. Am. Chem. Soc.* **121,** 8389 (1999).
12. A. Choudhury, S. Natarajan, and C. N. R. Rao, *Inorg. Chem.* **39,** 4295 (2000).
13. Crystal data: $(C_{10}N_4H_{28})_{0.5}[Zn(HPO_4)_2]\cdot 2H_2O$, orthorhombic, $a = 8.374(1)$ Å, $b = 15.270(2)$ Å, $c = 22.649(3)$ Å, $Z = 8$. Y.-P. Chiang and K.-H. Lii, unpublished results.
14. I. D. Brown and D. Altermatt, *Acta Crystallogr. Sect. B* **41,** 244 (1985).
15. G. M. Sheldrick, "SHELXTL Programs, Version 5.1." Bruker AXS, 1998.
16. A. E. Bennett, J. H. Ok, and R. G. Griffin, *J. Chem. Phys.* **96,** 8624 (1992).
17. D. Marion and K. Wuthrich, *Biochem. Biophys. Res. Commun.* **113,** 467 (1983).
18. S. Neeraj, S. Natarajan, and C. N. R. Rao, *Chem. Commun.* 165 (1999).
19. K. O. Kongshaug, H. Fjellvag, and K. P. Lillerud, *Solid State Sci.* **2,** 569 (2000).
20. C. N. R. Rao, S. Natarajan, A. Choudhury, S. Neeraj, and A. A. Ayi, *Acc. Chem. Res.* **34,** 80 (2000).
21. P. Reinert, A. Khatyr, B. Marler, and J. Patarin, *Eur. J. Solid State Inorg. Chem.* **34,** 1211 (1997).
22. P. Reinert, N. Zabukovec Logar, J. Patarin, and V. Kaucic, *Eur. J. Solid State Inorg. Chem.* **35,** 373 (1998).
23. M. Mehring, "Principles of High-Resolution NMR in Solids," 2nd ed. Springer-Verlag, Berlin, 1983.
24. W. Sommer, J. Gottwald, D. E. Demco, and H. W. Spiess, *J. Magn. Reson. A* **113,** 131 (1995).